Thermo-economic optimization of a 100 kW air-to-water heat pump for heating purposes in residential units

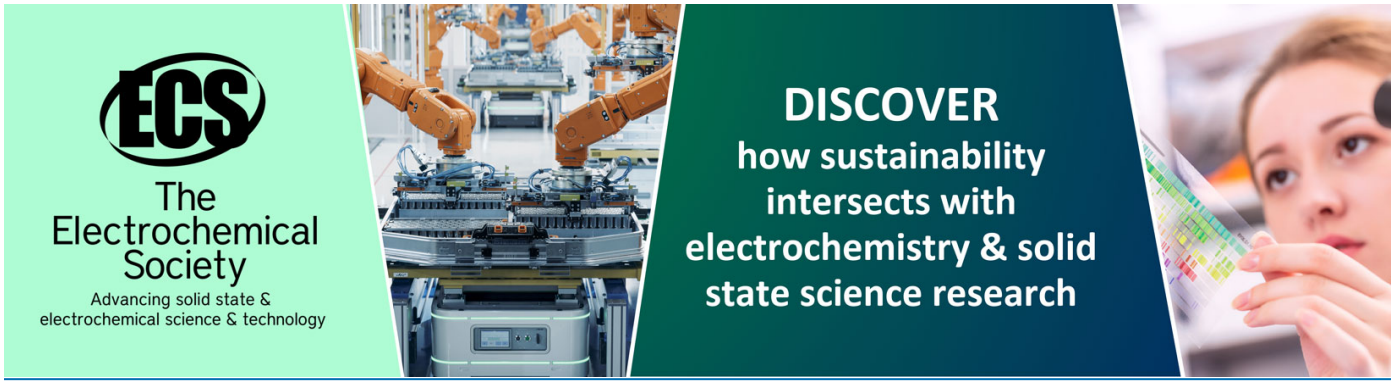

Thermo-economic optimization of a 100 kW air-to-water heat pump for heating purposes in residential units

I Viscardi[1], **L Viscito**[1], **L Del Ferraro**[2], **A W Mauro**[1]
[1] Department of Industrial Engineering, Federico II University of Naples, P.le Tecchio 80, 80125 Naples, Italy
[2] Daikin Applied Europe, Via Piani di S. Maria, 72, 00040 Rome, Italy

*Corresponding author: wmauro@unina.it

Abstract. In order to reach the ambitious objectives of carbon neutrality by 2050 and the limitation of the ambient temperature rise at 1.5 °C, several intensive energy fields such as heating and cooling appliances should be decarbonized. On this regard, electric heat pumps represent the most promising solutions to replace old and inefficient conventional boilers and comply with the ecological transition through the increase of electric energy production by means of renewable sources. In this paper, a thermo-economic optimization analysis of a 100 kW air-to-water electric heat pump is proposed. The appliance is designed to produce hot water at 55 °C. The developed model employs phenomenological equations calibrated on real data and manufacturer datasheets for compressor, heat exchangers, and costs. Different design options, including the heat exchangers size and the choice of the working fluid (among R32, propane R290, ammonia R717, R454C), are presented and discussed. The Pareto analysis is then employed to find the best possible configurations in terms of costs and performance.

1. Introduction

Reaching carbon neutrality by 2050 and limiting the ambient temperature rise to 1.5°C represent the challenges proposed from the COP26 conference [1]. In order to comply, aligning with the Net Zero Scenario milestones, a rapid acceleration of the rate of improvement for several fields is required, including the cooling and heating sectors. Focusing especially on the heating one, according to the IEA [2] and the European Union, electrical heat pumps play a significant role in the energy transition. They represent the most promising solutions to decarbonize the heating sector, replacing old and conventional appliances and increasing electric energy production from renewable sources. Moreover, heat pumps' new role is reflected in unprecedented growth. Sales in 2022 were up 38%, with about 3 million heat pumps sold. The total number of connected heating heat pumps is now around 20 million, in about 16% of European residential and commercial buildings.

In particular, the building sector on its own accounts for about 40 % of the total energy consumption, and the domestic hot water demand contributes as an important section of energy consumption in the residential building, especially in cold regions [2, 3].

Air source heat pumps, as their high energy conversion efficiency and emission reduction ability, are considered as an effective method to replace the electric water heaters, gas and fuel water heaters [4, 5].

The heat pump for domestic hot water production currently employs many HCFCs- and HFCs-based refrigerants, such as R410A (Global Warming Potential = 2088). However, according to the

Montreal Protocol and Kigali Amendment [6], their consumption and production will be gradually managed, making the utilization of low-GWP refrigerants quite critical.

In this context, the present work proposes a thermo-economic optimization analysis of a 100 kW air-to-water electric heat pump designed to obtain hot domestic water at 55°C. Four different refrigerant fluids are investigated: R32, R717, R290 and R454C (a mixture of R32 and R1234yf). For each fluid, different design variables for the heat exchangers are simulated thus evaluating the set-up costs for all the components and the performance of the appliance in terms of COP. From these results, a Pareto front is obtained and the optimum configuration is chosen as the best compromise between economic and performance parameters.

2. Case study description and method

Figure 1 provides a schematic of the modelled 100 kW air-to-water electric heat pump (a) and the related thermodynamic cycle on the T-s diagram (b) with R290.

The base plant is made up of a scroll compressor, a plate heat exchanger used as condenser, a thermostatic expansion valve and a fin and tube heat exchanger used as evaporator. The superheated vapor (point 1) is driven from the compressor to the first heat exchanger (point 2) in which the working fluid condenses. The saturated liquid (point 3) is laminated with a thermostatic valve (point 4) and it finally goes into the evaporator before closing the loop. The secondary fluids are water and air for the condenser and the evaporator, respectively.

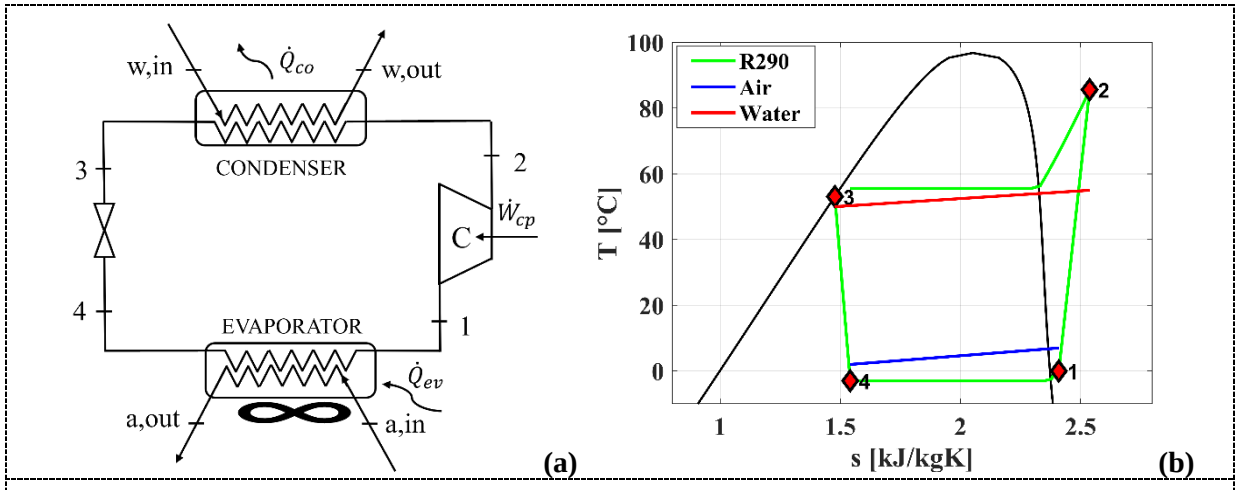

Figure 1. Electric heat pump schematic (a) and thermodynamic cycle (b) with R290 working in the following conditions: air evaporator inlet temperature $T_{a,in} = 7°C$, air evaporator outlet temperature $T_{a,out} = 2°C$, water condenser inlet temperature $T_{w,in} = 50°C$, water condenser outlet temperature $T_{w,out} = 55°C$, superheating $\Delta T_{sup} = 5°C$, subcooling $\Delta T_{sub} = 2.5°C$, evaporator pinch point temperature $\Delta T_{PP,ev} = 2°C$, condenser pinch point temperature $\Delta T_{PP,co} = 2°C$.

2.1. Compressor and valve modelling

A dedicated calibration of the global and the volumetric efficiency was carried out, by using the original data provided by the compressor manufacturer, thus obtaining the calculation of the electric power needed and the elaborated mass flow rate, according to equations (1) and (2) below. The parameter K is obtained through calibration, whereas n_0 represents the nominal rotating speed (3600 rpm) and f represents the ratio between the effective rotating speed and the nominal one. The trends of the global and volumetric efficiencies as functions of the compression ratio are shown in figure 2, (a) and (b) respectively:

$$\dot{W}_{cp} = \frac{\dot{m}_{cp} \cdot (h_{out,cp,is} - h_{in,cp})}{\eta_g} \quad (1)$$

$$\dot{m}_{cp} = \rho_{in} \cdot \eta_{vol} \cdot f \cdot \frac{n_0}{60} \cdot K \quad (2)$$

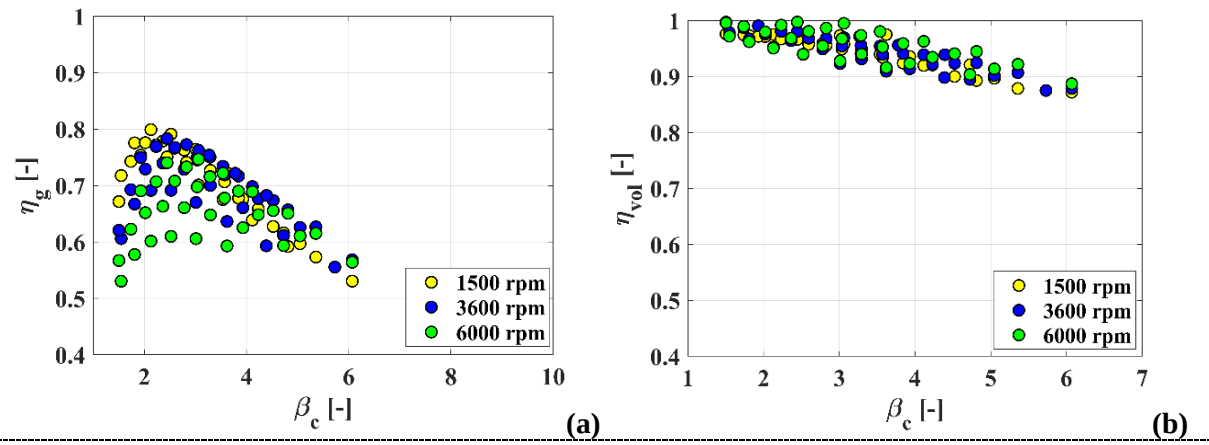

Figure 2. Global (a) and volumetric (b) efficiencies as a function of the compression ratio

As regards the thermostatic expansion valve, the hypothesis of an oversized device able to feed the compressor for any operating condition has been made.

2.2. Evaporator and condenser modelling

The evaporator is a fin and tube heat exchanger with the refrigerant passing inside the tubes and the air across tubes and fins. The materials employed are copper for the tubes (k_t= 390 $Wm^{-1}K^{-1}$) and aluminum for the fins (k_f= 230 $Wm^{-1}K^{-1}$) for all fluids except for ammonia (R717) for which stainless steel (k_t = 17 $Wm^{-1}K^{-1}$) is considered for tubes and aluminum for fins. This material is also employed for the plate heat exchanger employed as condenser.

The geometrical features and dimensions for both heat exchangers are shown in figure 3, where the elementary unit for the integration process is defined with black dotted lines:

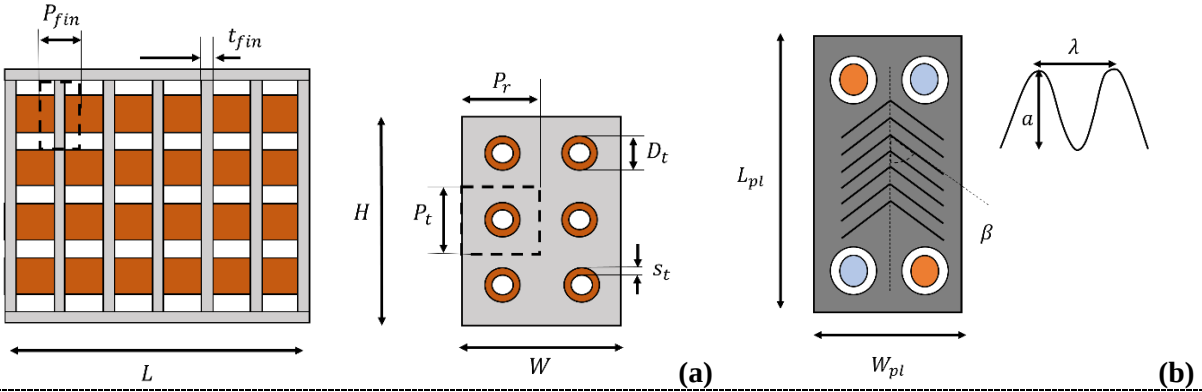

Figure 3. Evaporator (a) and condenser (b) geometrical features and parameters definition.

To calculate the heat transfer surface and its dimensions, the heat transfer equation is applied considering an elementary section:

$$\delta\dot{Q} = UdA \cdot \Delta T \tag{3}$$

The overall conductance UA is calculated by using the thermal resistances (convective and conductive ones) as shown in equation (4), where the subscripts *ev* and *air* refer to the evaporator while the subscripts *co* and *water* refer to the condenser:

$$UdA = \left(dR_{ref,ev/co} + dR_t + dR_{air/water}\right)^{-1} \tag{4}$$

Enthalpies and temperatures of the secondary fluid and of the refrigerant are then integrated with the energy balance over the length of the tube/plate, also considering the frictional pressure drop. As regards the evaporator fin and tube heat exchanger, the refrigerant flow is divided into several circuits (N_{circ}) working in parallel, and the calculation of the temperature profile is referred to a single circuit with the assumption that the refrigerant mass flow rate is the same in all circuits.

The heat transfer coefficient and the pressure drop of refrigerant and air/water are evaluated through dedicated prediction methods for each geometry. In particular, for the fin and tube evaporator, the fin efficiency and the air heat transfer coefficient are evaluated with the Wang et al. [7] model, while the refrigerant heat transfer coefficient is evaluated using the Gungor and Winterton [8] correlation during the boiling process and Dittus and Boelter [9] correlation for single phase calculations during superheating. The refrigerant pressure drop is calculated using the correlation of Muller-Steinhagen and Heck [10] for evaporating flow (and neglected for vapor single phase flow) whereas the air pressure drop is evaluated using the model of Wang et al. [7].

For the plate condenser, the water heat transfer coefficient is evaluated through the correlation of Martin [11]. Desuperheating and subcooling refrigerant heat transfer coefficients are calculated with Dittus and Boelter [9] correlation, whereas Shah et al. [12] method is employed for the condensing flow. The frictional pressure drops are neglected for water, whereas they are calculated with the Amalfi et al. [13] prediction method in case of refrigerant two-phase flow.

The iterative calculation for both heat exchangers starts at the first row/plate and the models add other row/plates if the thermal power evaluated is below its project value. By considering N_{el} elementary section for each row/plate and N_r/N_{pl}, the total thermal power is evaluable as follows:

$$\dot{Q}_{ev} = N_{circ} \cdot \sum_{j=1}^{N_{el}} \sum_{n=1}^{N_r} \dot{Q}_{n,j} \tag{5}$$

$$\dot{Q}_{co} = \sum_{i=1}^{N_{el}} \sum_{n=1}^{N_{pl}} \dot{Q}_{n,i} \tag{6}$$

If the calculated transferred heat is equal or above the design value, the algorithm stops the iterations along the elements without adding further rows/plates.

Finally, the electrical power consumption of the evaporator fan is obtained through the evaluation of the air pressure drop and fan efficiency (fixed at 0.45) as shown in equation (5):

$$\dot{W}_{fan} = \frac{\Delta P_{air} \cdot \dot{V}_{air}}{\eta_{fan}} \tag{7}$$

3. Resolution algorithm

The properties of the refrigerants are obtained through the software Refprop 10.1 [14]. The model has been numerically implemented in MATLAB [15] and the algorithm steps are the following:

- The thermodynamic cycle is evaluated using the following input data: air evaporator inlet temperature ($T_{a,in}$), water condenser inlet temperature ($T_{w,out}$), water condenser outlet temperature ($T_{w,out}$), superheating (ΔT_{sup}), subcooling (ΔT_{sub}) and the condenser thermal power ($\dot{Q}_{co}$). The exact values are all fixed and decision variables are shown in the following section, in table 1. An iterative procedure combined with the compressor model are used to calculate the condensation temperature (T_{co}), the compressor mass flow rate ($\dot{m}_{cp}$) and the condenser water flow rate ($\dot{m}_w$). The evaporator heat capacity $\dot{Q}_{ev}$ and the compressor power consumption $\dot{W}_{cp}$ are evaluated.
- Once the thermodynamic cycle is defined, the submodels related to both condenser and evaporator are used to define the size of the heat exchangers (in terms of number of rows N_r and circuits N_{circ} in the evaporator and number of plates N_{pl} in the condenser) that fits the needed design thermal power, for each geometrical configuration (see the specification in the following section, table 2). Before the calculation process, all the solutions that violate the constraints about the maximum height and length for the evaporator are discarded. The same applies to the solutions that violate the constraint on refrigerant pressure drop for the condenser and the one on the discharge temperature of the compressor.
- The COP as shown in equation (6), together with the set-up costs, whose functions are shown in the following section, table 3:

$$COP = \frac{\dot{Q}_{co}}{\dot{W}_{cp} + \dot{W}_{fan}} \tag{8}$$

4. Results

4.1. Operating conditions, geometrical parameters, cost functions and constraints

Thermodynamic boundary conditions, ranges and constraints for the vapor compression cycles, as well as the geometry of the evaporator and the condenser, are shown in table 1, table 2 and table 3. The size of the electric heat pump is 100 kW, working at nominal conditions heating water from 50°C to 55°C at the outlet of the condenser. The design ambient temperature and relative humidity are 7°C and 70%, respectively. Four different fluids, R32, R290, R717, R454C, are investigated.

The refrigerant pressure drops limits in heat exchangers are fixed to 2 °C (corresponding up to 2.0 bar), in order avoid higher compressor power consumption.

Table 1. Operating conditions and constraints for the thermodynamic cycle.

Parameter	Values/ranges
Fixed parameters	
Condenser thermal power, $\dot{Q}_{co}$	100 [kW]
Air evaporator inlet temperature, $T_{a,in}$	7 [°C]
Water condenser inlet temperature, $T_{w,in}$	50 [°C]
Water condenser outlet temperature, $T_{w,out}$	55 [°C]
Outlet evaporator superheating value, ΔT_{sup}	5 [°C]
Outlet condenser subcooling value, ΔT_{sub}	2.5 [°C]
Air evaporator inlet relative humidity, $\phi_{ev,in}$	0.7
Air velocity, w_a	4 [m/s]
Fan efficiency, η_{fan}	0.45 [-]
Variable parameters	

fluid	[R32 R290 R717 R454C]
Evaporator pinch point temperature variation, $\Delta T_{PP,ev}$	[5 7 9 10] [°C]
Condenser pinch point temperature variation, $\Delta T_{PP,co}$	[2 4 6] [°C]
Air temperature variation, ΔT_a	[5 7.5 10] [°C]
Maximum values of the constrained parameters	
Compressor discharge temperature	150 [°C]
Evaporator refrigerant pressure drop (in terms of temperature glide)	2 [°C]
Condenser refrigerant pressure drop (in terms of temperature glide)	2 [°C]

Table 2. Values of fin and tube and plate heat exchangers geometry data and their ranges.

Fin and tube heat exchanger		Plate heat exchanger	
Parameter	Values/ranges	Parameter	Values/ranges
Fixed parameters		**Fixed parameters**	
Fin thickness, t_{fin}	0.1 [mm]	Plate chevron angle, β	65 [°]
Fin louver height, L_h	0.95 [mm]	Corrugation depth, a	9 [mm]
Fin louver lenght, L_p	1.3 [mm]	Corrugation pitch, λ	4 [mm]
Evaporator length, L	2000 [mm]	Water collector diameter, D_p	24 [mm]
Evaporator height, H	1.115 [mm]	Plate thickness, s_{pl}	6 [mm]
Variable parameters		**Variable parameters**	
Tube thickness, s_t	[0.2 0.24 0.26 0.3] [mm]	Plate width, W_{pl}	[328 596 700] [mm]
External tube diameter, D_t	[5 7 7.94 9.52] [mm]	Plate length, L_{pl}	[754 908 1400] [mm]
Tube pitch, P_t	[19 22 24] [mm]	Plate pitch, b_{pl}	[1.8 1.26 0.7] [mm]
Row pitch, P_r	[19 22] [mm]		
Fin pitch, P_{fin}	[1.41 1.59 1.81] [mm]		

Table 3. Cost functions employed in this study for each of the system component.

Component	Cost function	Notes	Reference
Compressor	$52.63 \cdot \dot{V}_{cp} \cdot 1.2$ [€]	$\dot{V}_{cp}$ in m^3/h	Botticella et al. [16]
Expansion valve	$114.5 \cdot \dot{m}$ [$]	$\dot{m}$ in kg/s	Sanaye and Shirazi [17]
Fin and tube heat exchanger	$A_{ev,a} \cdot 45$ [€]	$A_{ev,a}$ in m^2	Botticella et al. [16]
Plate heat exchanger	$516.62 \cdot A_{ev,co,w} + 268.45$ [$]	$A_{ev,co,w}$ in m^2	Sanaye and Shirazi [17]

4.2. Optimization results

In figure 4 it is possible to observe the clouds of dots representing the simulated solutions for each refrigerant fluid (R32, R717, R290 and R454C) and their Pareto front. The set-up costs are put in non-dimensional form due to the commercial confidentiality.

R290 simulated solutions are the ones that show the highest value in terms of COP but also the highest ones in terms of set-up costs. This happens because for some configurations the condenser requires a higher number of plates, raising its set-up cost, and at the same time they present a higher value of the compressor global efficiency η_g, improving the COP value.

On the contrary, R454C simulated solutions show the lowest values in terms of COP because of low compressor global efficiency values and quite high set-up costs.

R32 simulated solutions show the most homogeneous distribution compared to the other fluids, with a COP value ranging approximately from 2 to 2.85 and non-dimensional set-up costs ranging from about 0.159 to 0.898. Finally, R717 simulated solutions appear to be completely contained by other refrigerants solutions.

For each Pareto front, an optimum configuration is found, however the one configuration that returns the optimum values in terms of COP and set-up costs is found for R32. This solution presents a COP value equal to 2.81 and non-dimensional set-up costs value of 0.217. The values of the variable parameters of the thermodynamic cycle and heat exchangers geometry for the optimum configuration are displayed in table 4. This optimum configuration is found working at nominal conditions heating water from 50°C to 55°C at the outlet of the condenser with ambient temperature equal to 7°C and a relative humidity of 70%. In order to evaluate the seasonal coefficient of performance SCOP and the running costs, the dynamic behavior of the appliance should be studied.

It is important to point out that a considerable number of configurations for R32 and for R717 have been discarded because they provided a very high temperature at the compressor outlet (>150°C). For these solutions, a liquid injection and/or another plant should be employed in order to practically consider them as possible results.

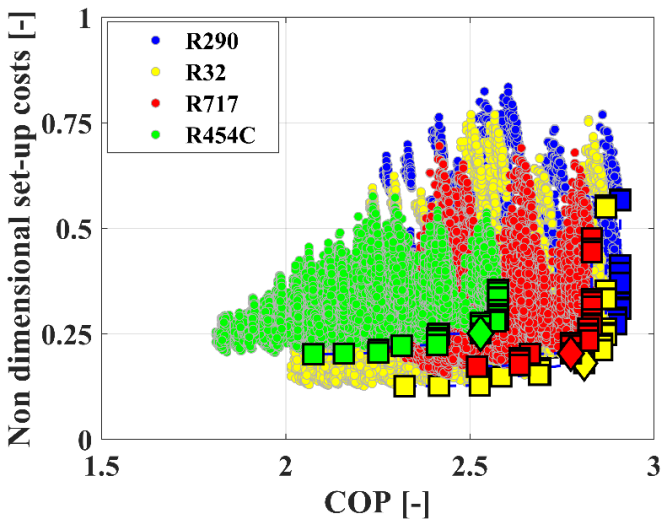

Figure 4. Pareto front showing COP versus non-dimensional set-up costs for different fluids.

Table 4. Values of the variable parameters of the thermodynamic cycle and heat exchangers geometry for the optimum configuration in terms of set-un costs and COP.

Thermodynamic cycle				
Fluid	**$\Delta T_{PP,ev}$ [°C]**	**$\Delta T_{PP,c}$ [°C]**	**ΔT_a [°C]**	
R32	5	5	2	
Fin and tube heat exchanger				
s_t [mm]	**D_t [mm]**	**P_t [mm]**	**P_r [mm]**	**P_{fin} [mm]**
3	9.52	24	19	1.81
Plate heat exchanger				
W_{pl} [mm]	**L_{pl} [mm]**	**b_{pl} [mm]**		

328	1400	0.7

Set-up costs [-]	**COP [-]**
0.217	2.81

5. Conclusions

In this work, a thermo-economic optimization analysis of a 100 kW air-to-water electric heat pump to produce hot water at 55 °C at ambient temperature and relative humidity of 7°C and 70%, respectively, has been carried out. Different conditions have been explored in terms of working fluid (R32, R717, R290 and R454C) and evaporator and condenser designs.

The main findings of the thermo-economic analysis are listed below:

- Among the simulated solutions, many of them have been discarded for R32 and R717 due to the very high compressor discharge temperature (>150°C). Alternative layout of the heat pump and/or the use of liquid injection should be explored to consider them as potential solutions.
- R290 simulated solutions show the highest value in terms of COP and set-up costs.
- R454C simulated solutions show the lowest values in terms of COP and quite high overall set-up costs.
- R32 proved to be the refrigerant fluid for which the optimum configuration is found. The non-dimensional set-up costs and the COP for the optimum configuration working at nominal conditions are equal to 0.217. and 2.81, respectively. To evaluate the seasonal optimum in terms of SCOP and in terms of running costs, the dynamic behaviour of the appliance should be investigated and will be part of future developments of the present work.

References

[1] COP26 Presidency Outcomes The Glasgow Climate Pact. November 2021 Glasgow (https://ukcop26.org/wp-content/uploads/2021/11/COP26-Presidency-Outcomes-The-Climate-Pact.pdf)
[2] International Energy Agency 2013 Transition to sustainable buildings: strategies and opportunities to 2050 Organization for Economic
[3] Rouleau J, Gosselin L, Blanchet P 2018 *Energy* **145** 677–90
[4] Guo X and Goumba A P 2018 *Energy* **164** 794–802
[5] Clauß J, Stinner S, Sartori I, Georges L 2019 *Appl. Energy* **237** 500–18
[6] Heath E 2017 *Int. Legal Mater* **56** 193-205
[7] Wang C C, Lee C J, Chang C T, Lin S P 1999 *Int. J. Heat Mass Transfer* **42** 1945–1956
[8] Gungor K E and Winterton R H S 1986 *Int. J. Heat Mass Transfer* **29** 351–358
[9] Dittus F W and Boelter L M K 1930 *Univ. California Publ. Eng.* **2** 443–461
[10] Müller-Steinhagen H and Heck K 1986 *Chem. Eng. Process Process Intensif* **20** 297**–**308
[11] Martin H 1996 Chemical Engineering and Processing: Process Intensification 35 **4** 301-310
[12] Shah M M, 1979 *Int. J. Heat Mass Transfer*. **22** 547–556
[13] Amalfi R L, Vakili-Farahani F, Thome J R 2016 *Int. J. Refrig* **61** 185-203
[14] Lemmon E W, Mc Linden M O, Huber M L 2009 REFPROP NIST Database 23
[15] MATLAB 2021b Release *Mathworks*
[16] Botticella F, De Rossi F, Mauro A W, Vanoli G P, Viscito L 2018. *Int. J. Refrig.* **87** 131–153
[17] Sanaye S and Shirazi A 2013 *Energ. Buildings* **60** 100–109